IEEE Access
Multidisciplinary | Rapid Review | Open Access Journal

Received December 17, 2019, accepted December 30, 2019, date of publication January 13, 2020, date of current version July 23, 2020.

Digital Object Identifier 10.1109/ACCESS.2020.2966053

Maximum Power Extraction Strategy for Variable Speed Wind Turbine System via Neuro-Adaptive Generalized Global Sliding Mode Controller

IZHAR UL HAQ[1], QUDRAT KHAN[2], (Member, IEEE), ILYAS KHAN[3], RINI AKMELIAWATI[4], KOTTAKKARAN SOOPY NISAR[5], AND IMRAN KHAN[6]

[1]Department of Electrical and Computer Engineering, COMSATS University Islamabad, Islamabad 45550, Pakistan
[2]Center for Advanced Studies in Telecommunications (CAST), COMSATS University Islamabad, Islamabad 45550, Pakistan
[3]Faculty of Mathematics and Statistics, Ton Duc Thang University, Ho Chi Minh City 758307, Vietnam
[4]School of Mechanical Engineering, The University of Adelaide, Adelaide, SA 5005, Australia
[5]Department of Mathematics, College of Arts and Science, Prince Sattam bin Abdul aziz University, Wadi Al-Dawaser 11991, Saudi Arabia
[6]Department of Electrical Engineering, College of Engineering and Technology, University of Sargodha, Sargodha 40100, Pakistan

Corresponding author: Ilyas Khan (ilyaskhan@tdtu.edu.vn)

ABSTRACT The development and improvements in wind energy conversion systems (WECSs) are intensively focused these days because of its environment friendly nature. One of the attractive development is the maximum power extraction (MPE) subject to variations in wind speed. This paper has addressed the MPE in the presence of wind speed and parametric variation. This objective is met by designing a generalized global sliding mode control (GGSMC) for the tracking of wind turbine speed. The nonlinear drift terms and input channels, which generally evolves under uncertainties, are estimated using feed forward neural networks (FFNNs). The designed GGSMC algorithm enforced sliding mode from initial time with suppressed chattering. Therefore, the overall maximum power point tracking (MPPT) control is very robust from the start of the process which is always demanded in every practical scenario. The closed loop stability analysis, of the proposed design is rigorously presented and the simulations are carried out to authenticate the robust MPE.

INDEX TERMS Feed forward neural networks (FFNNs), generalized global sliding mode controller (GGSMC), maximum power point tracking (MPPT), permanent magnet synchronous generator (PMSG), wind energy conversion systems (WECSs).

I. INTRODUCTION

Due to industrialization and increasing usage of electrical devices, the energy demand is increasing every day. Fossil fuels, which are becoming scarce nowadays are the main cause of global warming. Therefore the world energy experts investigate an alternate efficient and environment friendly energy resources. Wind energy, which is one of the investigated resource, attracted great attention because of its safety and cleanliness [1]. At the end of 2017, 52 giga watt (GW) of wind energy was added to the global installed capacity, and made a total of 539 GW [2].

The WECSs, based on speed, are categorized as fixed speed and variable speed WECs. In the fixed speed WECSs, the generator speed remains constant and they are connected to the grid without using power converters. In variable speed WECSs, the speed of the generator is continuously adopted and controlled in such a manner that the turbine always operates at its maximum efficiency. Consequently, the MPE phenomena occurs which increased the annual product by 5-10% [3]. Note that, the operating region of wind turbine is divided into four regions as depicted in Fig. 4. Region 1 covers operation from the startup to the cut-in speed. The sub operated region, called Region 2, is from cut-in to rated speed. In Region 3, the speed regulation region, the goal is speed regulation at rated levels because the wind speed remains high enough to drive the generator at its rated output power. Region 4 occurs after the cut-out speed in which the turbine is shut down to avoid any damage because of high wind speed [4]. It is worthy to note that maximum power can be extracted from the WECSs by operating the turbine in the starting and rated wind speed.

WECSs, equipped with variable speed permanent magnet synchronous generator (VS-PMSG), are becoming popular

The associate editor coordinating the review of this manuscript and approving it for publication was Ding Zhai.

day by day because of its higher efficiency, low weight, less maintenance, easy to control and no need for reactive and magnetizing current [5], [6]. The PMSG are generally operated by using a drive train technology [7] which builds coupling between the wind turbine and PMSG. In WECSs different power electronic converter with different topologies have been used to connect the generator (i.e PMSG) to the grid. These power interfaces, work as control unit for the MPE and build grids connection capability [8].

WECSs observe low cost installation with environment friendly nature, but suffer from low-efficiency due to varying wind speed. To increase the efficiency, they must be operated at the maximum power point (MPP). Thus MPP performs as an important part of a WECS. Sufficient work is done in the development of efficient MPPT controllers. Numerous MPPT control techniques are used for VS-PMSG which make it possible to continuously adapt the rotational speed of VS-PMSG relative to the wind speed. This resulted in enhanced efficiency of wind turbine with decreased power fluctuations [9], [10]. In MPPT one search for the maximum coefficient of performance (C_p) subjected to varying wind speed. Two broad categories i.e conventional design and soft computing design strategy, for the MPPT design, one focused extensively in the existing literature.

Among the conventional techniques, perturbation and observation (P&O) or hill climbing search (HCS) is the simplest (see for details [11]). The drawbacks of this method is that it does not work well for fast varying wind speed as well as for large inertia wind turbines [12]. The selection of optimum step size is also a difficult job in this method.

Thus researchers were fascinated by soft computing techniques which are classified as Bio-inspired methods and artificial intelligence (AI) methods. The Bio-inspired techniques includes particle swarm optimization (PSO) [13], ant colony optimization (ACO) [14] and genetic algorithms (GA) [15]. These MPPT controllers under varying wind speed, showed fast convergence as compared to conventional methods. However these methods need many parameters such as population size, mutation, selection of chromosomes and crossover rate. In addition, the estimation of these parameters is itself a complex job. Under varying wind speed, all these parameters need to be readjusted, otherwise one cannot track MPP correctly.

The AI strategies, for the MPPT of WECSs, include fuzzy logic (FL) based [16], [17] controllers and artificial neural networks (ANN) [18], [19]. These techniques work with variable inputs, without exact mathematical modelling along with self convergence and self learning capabilities. On addition they have adaptive nature for nonlinear behavior of the systems. The FL method [16], [17] harvested maximum power from the wind but the dependency of the tracking performance and output efficiency on the engineer's technical knowledge and the rules base table reduces its applicability. It also needs a lot of theoretical knowldge and may not guarantee an optimal response. The ANN [18] was employed for pitch controller design for a grid connected wind turbine system to harvest maximum power from available wind. Its performance was superior to conventional controllers. The ANN based MPPT controllers have better performance and effectiveness than the conventional and bio-inspired techniques. However, this requires months for training because of large memory size. In addition, it needs periodic tuning with the passage of time.

Other control techniques like proportional integral (PI) [20], quantitative feedback theory (QFT) [21] and Linear-quadratic-Gaussian (LQG) control technique [22] are also used for the MPPT of WECSs. All these techniques required a lot of computational and graphical analysis and have oscillating output power due to its non-robust nature.

Sliding mode control (SMC), introduced in 1950s, is famous for its versatile nature because it can be employed to both linear and nonlinear systems. It is also famous for its robust nature which is always claimed in sliding mode with reduced order dynamics. The order reduction, in sliding mode, provides insensitivity to parametric variations and disturbance of matched kind. It also demonstrates finite time convergence with good dynamic behavior and simple implementation [23], [24]. In order to deal with the unmatched uncertainties effects, an SMC strategy was synthesized with an uncertainty observer in [25] which showed very good results. In the context of intelligent designs, an SMC along with fuzzy logic was presented for uncertain descripter systems in [26]–[28]. It is important to report here that very impressive but summarized developments in SMC, technical research issues and future perspectives regarding the SMC, are presented in [29], [30]. Having witnessed very appelaing developments, the theory of SMC and its applications are still focused areas among the researchers. In the context of applications to power systems, a direct power control (DPC) based on SMC was proposed for the grid connected WECS in [31]. When the grid voltages becomes unbalanced then the SMC controller regulate the instantaneous active and reactive powers directly in stator stationary reference frame. To improve the control efciency and performance of SMC used in PMSG-based WECS an exponential reaching law, a necessary part of the sliding mode controller, was proposed in [32]. Since, the dynamics of the wind power system is very stochastic and uncertain, therefore, an adaptive second-order SMC was presented in [33]. This work dealt efectively the presence of model uncertainties and the intrinsic nonlinear behavior of WECS. A proportional integral type sliding surface based SMC was proposed for renewable energy conversion systems and the electric motor drives in [34], [35]. At this stage, in the context of SMC applications to power systems, we want to attract the focuss of the readers to an important point that conventional SMC experiences reaching phase which reduces the robustness property of the SMC and it also causes chattering across the sliding constraint. Different techniques have been used to eliminate the reaching phase and to reduce the chattering effects (see for instance [36]). Since the amplitude of chattering phenomena is generally proportional to the amplitude of unknown dynamics e.g drift terms, input channels and disturbances. Therefore, in this work,

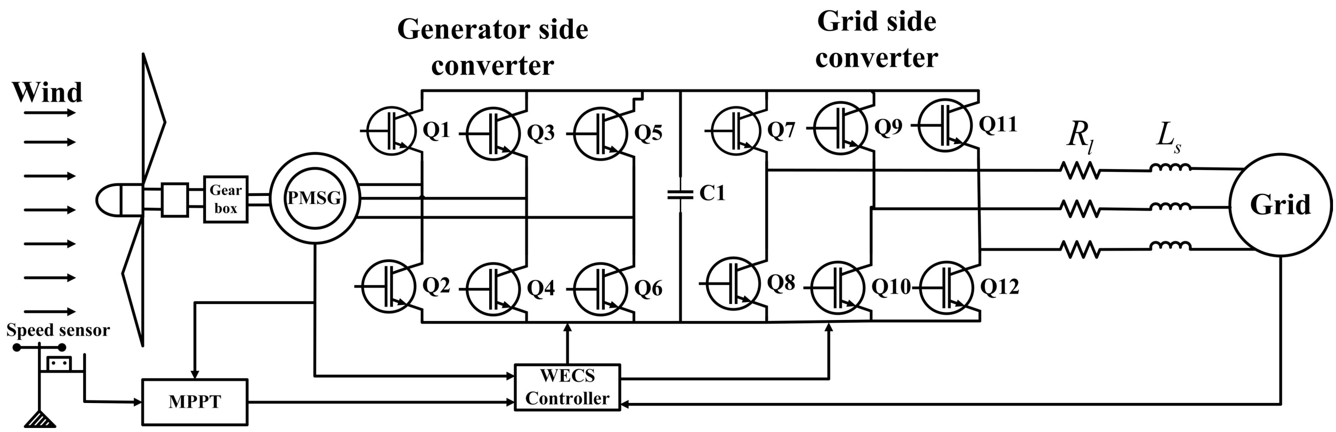

FIGURE 1. Wind energy conversion system.

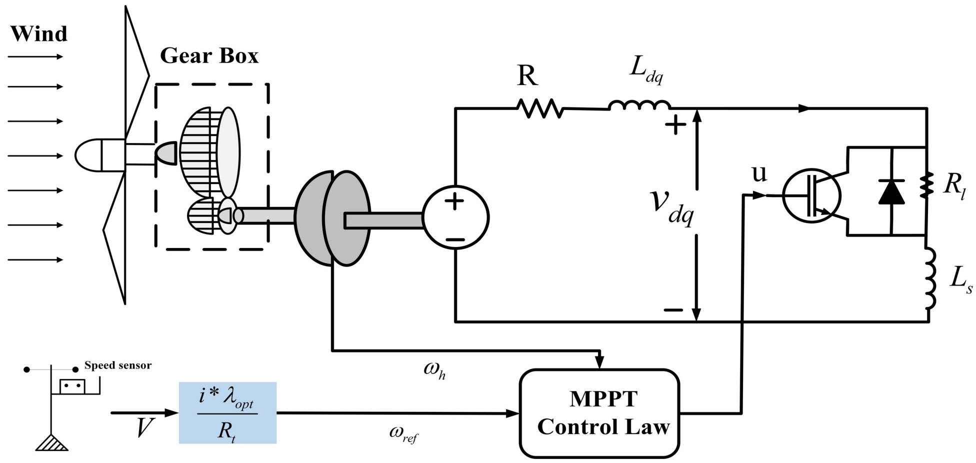

FIGURE 2. Equivalent model of WECS.

the uncertain nonlinearities (i.e drift terms and input channel) are accurately estimated via the FFNNs. Consequently, the chattering is suppressed because the uncertainty bound (for a sliding mode) will be a bit smaller in this adaptive case. In addition, the surface across which the sliding mode is enforced is an integral type which also results in chattering suppression along with enhanced robustness. The chatterring suppression is also targeted via the use of a strong reachability law. The use of this reachability law gives us fast sliding mode enforcement time. The elimination of reaching phase, which often results in decreased robustness, is also a target in this work. Therefore, a FFNNs based robust GGSM MPPT control law is developed in this paper which is quite fascinting to investigate. The closed loop stability analysis and states convergence is ensured mathematically and simulations (in MATLAB environment) are carried out to authenticate the claim. The developed results are also compared with standard literature results [37].

The rest of the paper is structured as follow. The detail of WECS is given in Section 2 and input-output form of the considered system is presented in Section 3. The FFNN, used for the estimation of unknown terms and analysis of the proposed control technique, is discussed in Section 4 and section 5 respectively. Simulation results under varying wind speed is given in Section 6. In Section 7, the performance of the proposed controller is compared with standard feedback linearization approach. Finally, the conclusion is presented in Section 7.

II. MODELLING OF WECS

The model of WECS which will be studied in this paper is shown in Fig. 1. It mainly consists of a turbine, a gear box, converters and a variable speed wind turbine which is equipped with a PMSG and is further connected to a grid. The system illustrated in Fig. 2, is an equivalent model of the system of Fig. 1. The variable resistance R_l and the constant inductance L_s are the control variables in which L_s is kept fixed and R_l is adjusted to extract maximum power.

Now the detailed presentation of wind turbine model, drive train and PMSG will be given in the following study.

A. WIND TURBINE MODEL

The fundamental equation governing the mechanical power captured by the turbine from wind is given as [38]:

$$P_{mech} = \frac{1}{2}\rho A V^3 C_p(\lambda, \beta) \tag{1}$$

where ρ is the air density (kg/m^3), C_p is the power coefficient, A is the area of the blades (m^2), V is the average wind speed (m/s), λ is the tip speed ratio and β is the pitch angle. As the wind speed increases the mechanical output power of wind turbine significantly increases as clearly seen in Fig. 3.

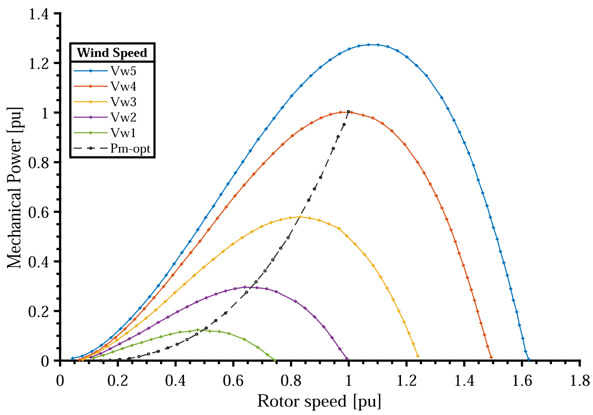

FIGURE 3. Wind turbine speed vs output mechanical power.

The tip speed ratio is defined as

$$\lambda = \frac{\omega_h R_t}{V} \tag{2}$$

where R_t is the radius of the turbine(m) and ω_h is the angular speed of the high speed shaft. Note that C_p is a nonlinear function of lambda λ and beta β, whose values varies from system to system. The detailed mathematical expression of C_p is given as [39]:

$$C_p = (0.5 - 0.0167(\beta - 2) sin[\frac{\pi(\lambda + 0.1)}{18 - 0.3(\beta - 2)}] - 0.00184(\lambda - 3)(\beta - 2) \tag{3}$$

The theoretical upper limit of C_p, also known is Betz coefficient, is 0.47 [40]. For different values of beta, the C_p characteristic curve is shown in Fig. 4. By changing λ and β, the C_p is changing. At a specific λ called lambda optimum (λ_{opt}) the value C_p is maximum which is called $C_{p\,max}$. By following the $C_{p\,max}$ curve, the variable speed wind turbine gets maximum power from the wind (i.e., by varying the rotor speed to keep the system at rated speed and λ_{opt}).

B. DRIVE TRAIN MODEL

By neglecting the stiffness and damping factor, the one-mass drive train model [37] is described as.

$$J\frac{\partial \omega_h}{\partial t} = T_a - T_{em} \tag{4}$$

where J is the inertia constant of the high speed shaft, T_a is the aerodynamic torque and T_{em} is the electromagnetic torque.

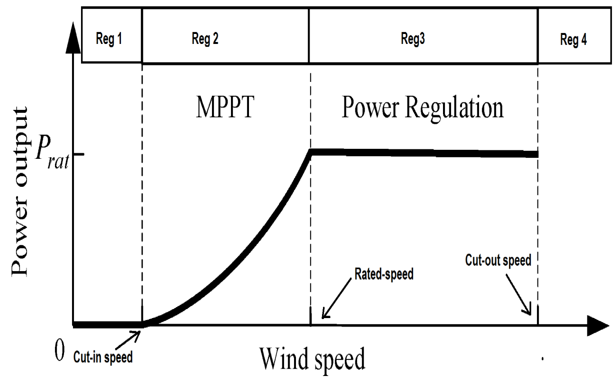

FIGURE 4. Wind turbine operation regions.

Note that the mechanical power, in term of T_a and ω_h, looks as follows

$$P_{mech} = T_a \omega_h \tag{5}$$

The ratio between C_p and λ appear as follows

$$C_q = \frac{C_p(\lambda, \beta)}{\lambda} \tag{6}$$

Incorporating (1) and (2) in (5), one may get

$$T_a = \frac{1}{2}(\rho \pi r^3) C_q V^2 \tag{7}$$

For the purposes of optimal control, the C_q in term of λ is approximated as follows

$$C_q(\lambda) = a_0 + a_1\lambda + a_2\lambda^2 \tag{8}$$

Using (2) in (8) and then incorporating it in (7), the aerodynamic torque T_a becomes

$$T_a = d_1 v^2 + d_2 v \omega_h + d_3 {\omega_h}^2 \tag{9}$$

where

$$d_1 = \frac{1}{2}\pi\rho R_t^3 a_0, \quad d_2 = \frac{1}{2}\pi\rho R_t^4 a_1, \quad d_3 = \frac{1}{2}\pi\rho R_t^5 a_2 \tag{10}$$

with

$$a_0 = 0.1253, \quad a_1 = -0.0047, \quad a_2 = -0.0005 \tag{11}$$

C. PMSG MODEL

Having performed Park's transformation and eliminating v_o, the PMSG model can be described by the following dynamics [37].

$$v_d = Ri_d + L_d\frac{di_d}{dt} - L_q i_q \omega_s \tag{12}$$

$$v_q = Ri_q + L_q\frac{di_q}{dt} + (L_d i_d + \phi_m)\omega_s \tag{13}$$

where R is the stator resistance, v_d, v_q are d and q stator voltages, L_d and L_q are the d and q inductances, ω_s is the stator pulsation and ϕ_m is the flux that is constant due to permanent magnets.

The electromagnetic torque is expressed as

$$T_{em} = p[\phi_m i_q + (L_d - Lq) i_d i_q] \tag{14}$$

where p is the number of pole pairs. If the permanant magnet is mounted on the rotor surface, then L_d becomes equal to L_q. Consequently,

$$T_{em} = p\phi_m i_q \tag{15}$$

The non linear equations for a PMSG, when connected to a grid, is described as [37]

$$\begin{cases} \dot{i}_d = -\dfrac{1}{L_d + L_s}[(R + R_l)i_d + p(L_q + L_s)i_q\omega_h] \\ \dot{i}_q = -\dfrac{1}{L_q + L_s}[(R + R_l)i_q - p(L_d + L_s)i_d\omega_h + p\phi_m\omega_h] \\ \dot{\omega}_h = \dfrac{1}{J}(T_a - p\phi_m i_q) \end{cases} \tag{16}$$

while R_l is the load resistance and L_s is the load inductance and ($\omega_h = \omega_l \times i$ and i is the gear ratio).

The system (16), in general form, can be expressed as

$$\begin{cases} \dot{x} = f(x) + g(x)u \\ y = h(x) \end{cases} \tag{17}$$

where i_d, i_q, and ω_h is considered as x_1, x_2, and x_3, respectively, and R_l is replaced with u. In addition,

$$\begin{cases} f(x) = \begin{bmatrix} \frac{1}{L_d+L_s}(-Rx_1 + p(L_q - L_s)x_2x_3 \\ \frac{1}{L_q+L_s}(-Rx_2 - p(L_d + L_s)x_1x_3) + p\phi_m x_3 \\ \frac{1}{J}(d_1v^2 + d_2vx_3 + d_3x_3^2 - p\phi_m x_2) \end{bmatrix} \\ \in I\!R^{3\times 1} \\ -g(x) = \begin{bmatrix} \frac{1}{L_d+L_s}x_1 \\ \frac{1}{L_q+L_s}x_2 \\ 0 \end{bmatrix} \in I\!R^{3\times 1}.u \\ \text{and } y = h(x) = x_3 = \omega_h \text{ is the output of the plant.} \end{cases} \tag{18}$$

III. INPUT-OUTPUT FORM

For our control strategy, the most suitable form is the input-output form of the (18) as in [37], [41] which is represented as by defining the following transformation.

$$\left.\begin{aligned} z_1 &= y = h(x) = x_3 = \omega_h \\ z_2 &= L_f h(x) = \frac{\partial h(x)}{\partial x}.f(x) = m_1 - m_2x_3 - m_3x_3^2 - m_4x_2 \\ z_3 &= L_f^2 h(x) = \frac{x_1}{x_2} \end{aligned}\right\} \tag{19}$$

Since the relative degree, r of the system is one, less than the system order n i.e., ($r < n$), so the input-output form appear as follows

$$\left.\begin{aligned} \dot{z}_1 &= z_2 \\ \dot{z}_2 &= L_f^2 h(x) + L_g L_f h(x)u \end{aligned}\right\} \tag{20}$$

$$\begin{aligned} \dot{z}_3 = \frac{m_4}{m_1}&(-\frac{k_1z_3m_1}{m_4} - \frac{k_2z_1m_1}{m_4} - \frac{k_3z_3m_1u}{m_4}) \\ &-(\frac{z_3m_1}{m_4})(\frac{m_4^2}{m_1^2})(-\frac{l_1m_1}{m_4} - \frac{l_2m_1z_3z_1}{m_4} + l_3z_1 - \frac{l_4m_1u}{m_4}) \end{aligned} \tag{21}$$

The parametric values of the under study model is given in table 1. The values of the derived parameters are calculated by using the typical parameters given in the table 2 and 3 (see for more details [37], [41]).

TABLE 1. Parametric values of the under study model.

Symbol	Value	Symbol	Value
k_1	27. 35028	k_2	-0. 94866
k_3	-8. 22639	l_1	-27. 14708
l_2	-3	l_3	1. 3146
l_4	-8. 22639	m_1	487. 4891
m_2	-0. 93297	m_3	-0. 00506
m_4	-23. 8152	d_1	3.8442
d_2	-0.3605	d_3	-0.0959

So, one of the transformed state i.e., z_3 is of zero dynamics. Now, it is necessary to discuss the stability of the zero-dynamics.

A. ZERO-DYNAMICS STABILITY INVESTIGATION

The nonlinear system's dynamics are divided into 2 parts i.e., an internal part and an external (input-output) part, when performing the input-output conversion. Since, the external dynamic states i.e., (z_1, z_2) are controllable states and are directly controlled by u while the stability of the internal dynamic state i.e., (z_3) is simply determined by the location of zeros called zero-dynamics for a nonlinear system [42]. To calculate the zero dynamics, the following variables should be set to zero i.e., $z_1 = z_2 = u = 0$ in (21). By simplifying (21), finally one gets

$$\dot{z}_3 = -z_3(k_1 - l_1) \tag{22}$$

where $k_1 > l_1$, so

$$\dot{z}_3 = -Kz_3 \tag{23}$$

where K is a positive integer. So the zero-dynamic state z_3 is stable as long as $k_1 > l_1$.

Remark 1: The third order nonlinear system (reported in (19)) with two visible states i.e., z_1, z_2 and one internal dynamics state z_3, is considered for the controller design which will be discussed in details in the control design section.

IV. UNKNOWN TERMS ESTIMATION

This section presents the estimation of the nonlinear drift term $L_f^2 h(x)$ and input channel $L_g L_f h(x)$ for the input-output form developed in the previous section. The estimation is done via FFNNs which will discussed below.

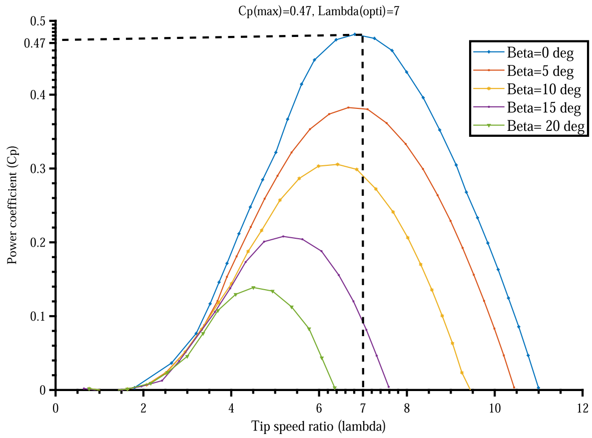

FIGURE 5. Characteristics curves of C_p by varying β.

A. ESTIMATION OF DRIFT TERM ($L_f^2 h(x)$) AND INPUT CHANNEL ($L_g L_f h(x)$)

In order to estimate the nonlinear mapping between the independent variables i.e., z_1, z_2, z_3 and V, and the depending variables $L_f^2 h(x)$ and $L_g L_f h(x)$, a FFNN is used [43]. The NNs learns to create a mapping between these independent variable and dependent output [44]. The training set in NNs for this nonlinear approximation will include the states z_1, z_2, z_3 and V. A three layer FFNN is an efficient method for the non-linear function estimation. The schematic diagram of under study procedure is shown in Fig. 6.

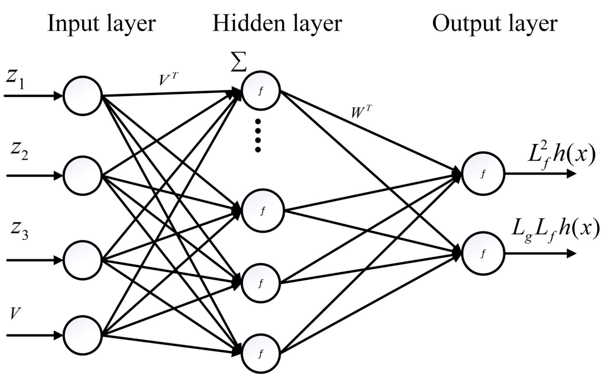

FIGURE 6. FFNN for $L_f^2 h(x)$ and $L_g L_f h(x)$ generation.

The informations in the input layer are multiplied by scalar weighted, V_{ij}, with a biased value b_{jo}. This input layer computes its net activation as

$$a_j = \sum_{i=1}^{n} V_{ji} p_i + b_{jo} \tag{24}$$

where $j = 1, 2, 3 \ldots, l_o$ represents the number of neurons in the hidden layer, p_i is the input of the input node i, b_{jo} is the respective reconstruction error or bias. The output of the hidden layer is given by

$$y_i = f(a_j) \tag{25}$$

where f is the activation function which is chosen to be tanh.

The output layer computes its net activation as follow

$$a_k = \sum_{j=1}^{l_o} \omega_{kj} y_i + b_{ko}, \tag{26}$$

where k is the number of neuron in the output layer, ω_{kj} is scalar called weight between the k^{th} output layer node and the j^{th} hidden layer node. The output layer produces an outputs $L_f^2 h(x)$ and $L_g L_f h(x)$ as a function of its net activation as follows

$$\begin{cases} L_f^2 h(x) = f_1(a_k) \\ L_g L_f h(x) = f_2(a_k) \end{cases} \tag{27}$$

The outputs of the estimated model can be expressed as the function of the inputs, the weights between input and hidden layer and the weights between the hidden and the output layer which is described as follows

$$\begin{cases} L_f^2 h(x) = f_1\left(\sum_{j=1}^{l_o} \omega_{kj} f\left(\sum_{i=1}^{n} V_{ji} p_i + b_{jo}\right) + b_{k0}\right) \\ L_g L_f h(x) = f_2\left(\sum_{j=1}^{l_o} \omega_{kj} f\left(\sum_{i=1}^{n} V_{ji} p_i + b_{jo}\right) + b_{k0}\right) \end{cases} \tag{28}$$

For two layer the FFNN, as shown in Fig. 6, consider l_o and k_1 are the number of neurons in layer1 and layer2, respectively. So, the above equations can also be presented in the vectors form as

$$L_f^2 h(x) \text{ or } L_g L_f h(x) = \bar{f}(\bar{W}^T \bar{f}(\bar{V}^T \bar{p} + b_v) + b_w) \tag{29}$$

More explicitly, this expression can be expressed as follows

$$L_f^2 h(x) \text{ or } L_g L_f h(x) = (W tanh(V\bar{p} + b_v) + b_w) \tag{30}$$

After selection of the network structure, the network training is done by minimizing the cost function. The cost function is generally characterized as follows

$$J(V_{ji}, \omega_{kj}) = \frac{1}{2} \sum_{i=1}^{l_o} (t_k - z_k)^2 \tag{31}$$

where t_k is the target output at the k^{th} output node and $J(V_{ji}, \omega_{kj})$ is the mean square error (MSE).

Levenberg-Marquardt training algorithm is used for updating the weights of the FFNN. The MSE criterion or the maximum number of iterations decide the termination of the iterative process. A range of values of the network parameters has been varied systematically to achieve a good estimate of the training data. The varying network parameters are the number of hidden neurons in the hidden layers, with learning rate range and the number of iterations are used for the estimation of $L_f^2 h(x)$ and $L_g L_f h(x)$.

The final FFNN structure for $L_f^2 h(x)$ and $L_g L_f h(x)$ has three layer and the learning rate is 0.1. The first layer consists of the inputs. The second layer which is the hidden layer consists of ten neurons with sigmoid function as an activation function. The third layer is an output layer which gives us

$L_f^2 h(x)$ and $L_g L_f h(x)$ as an estimates of the plant drift terms and input channel, respectively. This choice of the network parameters yields a good match between the actual and the predicted values.

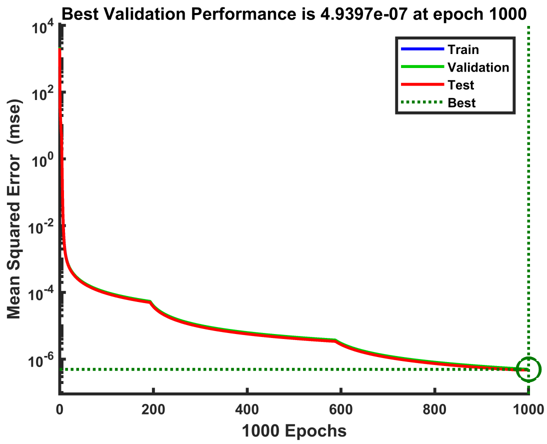

FIGURE 7. Performance plot.

1) SIMULATION RESULTS OF FFNN

The performance in terms of MSE, during the estimation of $L_f^2 h(x)$ and $L_g L_f h(x)$, is shown in Fig. 7. It the start there is considerable amount of error. However, with the increase in epoches, the error reduces to its minimum value. Their regression plots, depicted in Fig. 8, are plotted against the target values. The regression parameter R decides the success rate of estimation. If $R = 1$, it mean good estimates are made and as R decreases the true estimation decreases.

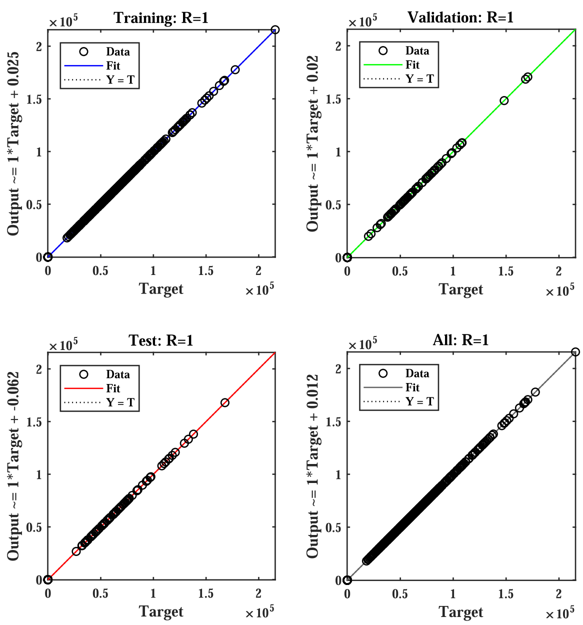

FIGURE 8. Regression plot.

The estimation error histogram associated with $L_f^2 h(x)$ and $L_g L_f h(x)$ shown in Fig. 9. It reveals a very small error with an average very close to zero.

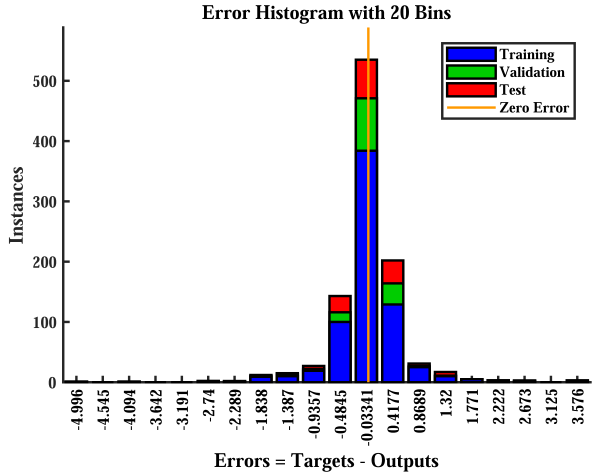

FIGURE 9. Mean squared error histogram.

This estimation provides the estimates ($L_f^2 h(x)$ and $L_g L_f h(x)$) which will be used in control algorithm outlined in next section.

V. GENERALIZED GLOBAL SLIDING MODE CONTROL

In this section the GGSMC based control law is designed to extract maximum power from the WECS. This job can be done by steering ω_h to ω_{opt} by logically varying the control input u (*i.e.*, R_l). Now, by considering the output based normal form (20) subject to uncertainties. Thus one may have

$$\begin{cases} \dot{z_1} = z_2 \\ \dot{z_2} = L_f^2 h(x) + L_g L_f h(x) u + \Delta(z_1, z_2, t) \end{cases} \tag{32}$$

where $z_1 = x_3$ and $z_2 = \frac{1}{J}(d_1 v^2 + d_2 v x_3 + d_3 x_3^2 - p\phi_m x_2)$ and $\Delta(z_1, z_2, t)$ is the uncertainty which is assumed to be matched and bounded by a positive constant K i.e., $|\Delta(z_1, z_2, t)| \leq \overline{K}$.

Since the ultimate objective is the tracking of the optimum speed of the generator named as ω_{opt}. Therefore, the mismatch between the actual and reference speed is defined by

$$e = z_1 - \omega_{ref} \tag{33}$$

where $\omega_{ref} = \omega_{opt}$ Based on this error, a new variable σ is defined as follows

$$\sigma = \dot{e} + ae - f(t) \tag{34}$$

where the function $f(t)$, called the forcing function, must be designed (according to [45]) to meet the following three conditions so that $\sigma = 0$ is satisfied for all $t \geq 0$.

1) $f(0) = \dot{e}_0 + ae_0$
2) $f(t) \to 0$ as $t \to \infty$
3) $f(t)$ has a bounded first time derivative

Here $\dot{e}_0$ and e_0 are the velocity and position errors respectively, at $t = 0$. The detailed mathematical expression of $f(t)$ in GGSMC is chosen as follows

$$f(t) = [(\dot{e}_0 + ae_0)cosbt - be_0 sinbt] \exp(-at) \tag{35}$$

where a and b are positive constants. Note that, this forcing function satisfy all the above three conditions.

when $\sigma = 0$ is met, then the solution of the closed loop system will be governed by the following differential equation $\dot{e} + ae - f(t) = 0$. The solution of this equation appears as follows

$$e(t) = (e_0 cosbt + \frac{\dot{e}_0 + ae_0}{b} sinbt) \exp(-at) \tag{36}$$

It is worthy to mention that this solution can also be obtained by solving the forthcoming second order system

$$\ddot{e} + 2a\dot{e} + (a^2 + b^2)e = 0 \tag{37}$$

with initial conditions $\dot{e}(0) = \dot{e}_0$ and $e(0) = e_0$.

The poles of this system are lying at $-a \pm bj$. This gives the indication that the dynamics of the system, in sliding mode, does not reduces which implies that the system experiences integral sliding mode for all $t \geq 0$.

The time derivative of (34) along system (32) becomes

$$\dot{\sigma} = \dot{z_2} - \ddot{\omega}_{opt} + c(\dot{z_1} - \dot{\omega}_{opt}) - \dot{f}(t) \tag{38}$$

At this stage, the main interest is that the system should evolves with full states. Thus, a proportional integral surface in term of σ can be defined as follows

$$\xi = \sigma + c \int_0^t \sigma(\tau) d\tau \tag{39}$$

The choice of such proportional integral surface carries very interesting meaning. This is actually a PI type manifold which provides us no order reduction (to the order of system's dynamics) in sliding mode. Consequently, the system evolves with full states in sliding mode from the very start which results in enhanced robustness. In addition, this type of surface accompanied by the strong reachability law (reported in equation (43)) results in the suppressed chattering phenomenon.

The time derivative of ξ becomes

$$\dot{\xi} = \dot{\sigma} + c\sigma \tag{40}$$

Now incorporating the values of σ and $\dot{\sigma}$ and then posing $\dot{\xi} = 0$ and then calculating for the input u, one may get

$$u_{equ} = \frac{1}{l_g l_f h}[-a(z_2 - \dot{\omega}_{opt}) - l^2 fh + \ddot{\omega}_{opt} + \dot{f}(t)] \tag{41}$$

Since the practical system always operates under uncertainties therefore, the equivalent control alone will be no more capable to enforce sliding mode. So, the overall sliding mode enforcement law appear as follows

$$u = u_{equ} + u_{dis} \tag{42}$$

where

$$u_{dis} = -k_1(\xi + Wsign(\xi)); \quad 0 < \mathrm{W} < 1. \tag{43}$$

The schematic diagram of the designed control technique is shown in Fig. 10.

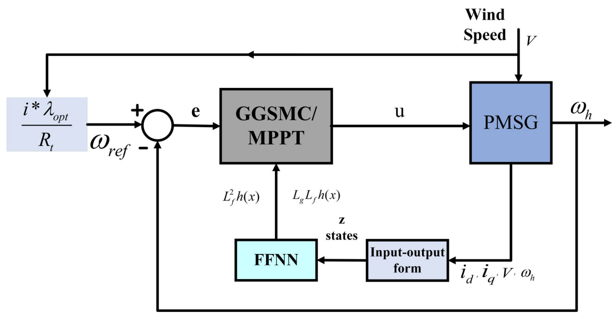

FIGURE 10. Control design for WECS equipped with PMSG.

Theorem 1: The sliding mode will be enforced along the manifold (39) by the control law of the (43) and hence the tracking will happen if the switching gain of the discontinuous control component ($i.e$, u_{dis}) chosen larger than the bound of the uncertainty i.e.,

$$K > |\Delta(z_1, z_2, t)| + \eta$$

Proof: Now, at this stage we are ready to confirm sliding mode establishment. A lyapunove function, in term of the sliding variable, is defined as follows.

$$V = \frac{1}{2}\xi^2 \tag{44}$$

The time derivative of this function along (41) becomes

$$\dot{V} = \xi\dot{\xi} = \xi(\dot{\sigma} + c\sigma) \tag{45}$$

Using (38) and (42) (with components given in (41) and (43)), one may get

$$\dot{V} = \xi(-k_1(\xi + Wsign(\xi)) + \Delta)$$

or

$$\dot{V} \leq -k_1\xi^2 - k_1 W|\xi| + |\xi||\Delta| \tag{46}$$

$$\dot{V} \leq -k_1\xi^2 - |\xi|(k_1 W - |\Delta|) \tag{47}$$

This expression remains true, i.e., negative definite, if

$$k_1 W - |\Delta| \geq \eta > 0$$

$$k_1 W \geq \eta + |\Delta| \tag{48}$$

The inequality (47) can also be written as

$$\dot{V} \leq -k_1 2V - \sqrt{2}\eta V^{\frac{1}{2}} \tag{49}$$

or

$$\dot{V} + k_1 2V + \sqrt{2}\eta V^{\frac{1}{2}} \leq 0 \tag{50}$$

The differential inequality is a fast finite time converging equation, which confirms that V approaches to zero in finite time. It means that ξ approaches to zero. As $\xi \longrightarrow 0$, the equation (40) becomes

$$\dot{\sigma} + c\sigma = 0 \tag{51}$$

The homogeneous equation has a solution

$$\sigma(t) = \sigma(0)exp(-at) \tag{52}$$

It means that σ will approach to zero. The σ convergence to zero certify the equation (37) with solution reported in (36). Thus, the tracking error converges to zero which in turn provide us the reference tracking. This proves the theorem. Having tracked the reference, the maximum power will be extracted via the equation (1).

VI. SIMULATION RESULTS AND DISCUSSIONS

In this section, the closed loop simulation results of the afore said process are displayed. In the first subsection the robust tracking performance in an uncertain scenario is performed while in the second subsection the comparison to standard literature results is shown.

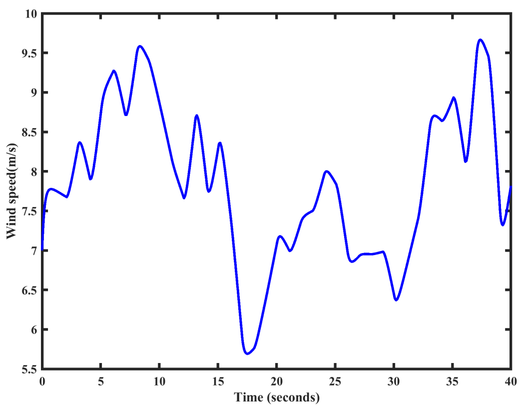

FIGURE 11. Wind speed profile.

TABLE 2. Parameters of wind turbine.

Parameter	Value
Air density ρ	$1.25\ kg/m^3$
Blade radius R_t	2.5 m
Maximum power coefficient C_p	0.47
The tip speed ratio λ (optimum value)	7

A. ROBUST TRACKING PERFORMANCE

The VS-WECS equipped with PMSG has been build based on equations (1) to (16). The power rating of the VS-WECS equipped with PMSG is 3 kilo Watt (kW). The wind speed profile is generated through Kaimal spectra is shown in Fig. 11 reported in [46]. The simulations has been performed using variable step ode45 solver. Different parameters of the wind turbine and PMSG are shown in table 2 and table 3 of Appendix, respectively. These parameters are adapted from [37]. In order to verify the tracking performances of the investigated controller, the simulation results are shown in Fig. 12-14. In Fig. 12, the tracking performance of the reference generator speed by the actual speed of the generator is ensured by GGSMC. In Fig. 13 and Fig. 14, power coefficient C_p and the tip speed ratio λ are displayed, respectively. The actual variations in C_p and λ can be seen in the zoomed sections of the Fig. 13 and 14. The C_p value was found very close to its optimum value of 0.47 where as the λ was found very closed to its optimum value 7.

TABLE 3. Parameters of PMSG.

Parameter	Value
The stator resistance R	3.3 Ω
d inductance	L_d=41.56mH
q inductance	L_q=41.56mH
Flux value	0.4382Wb
Pole pairs p	3

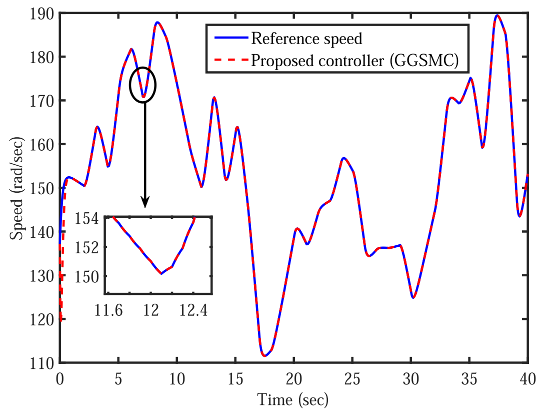

FIGURE 12. Reference speed tracking via shaft speed.

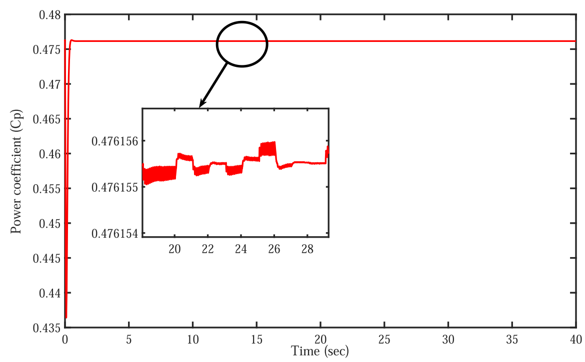

FIGURE 13. Power coefficient evolution.

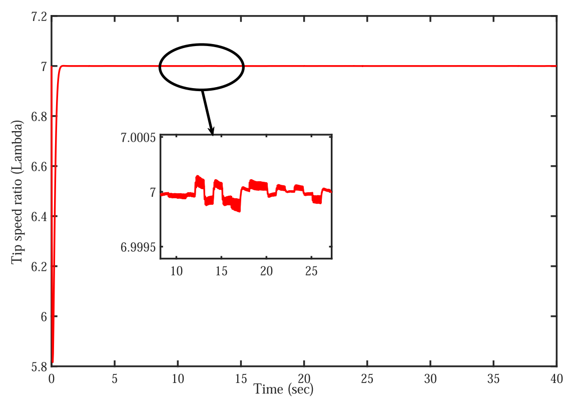

FIGURE 14. Tip speed ratio vs time.

It is important to mentioned that the wind speed tracking was performed in uncertain scenarios. The uncertainties of matched kind were $0.5sin(t)$ while the plant parameters were varied with a change of 5%. The performance is quit good and the maximum power is nicely extracted by keeping the power coefficient C_p and the tip speed ratio λ close to their optimum values. Hence the NNs base GGSMC displays its self as an appealing candidate for such power systems.

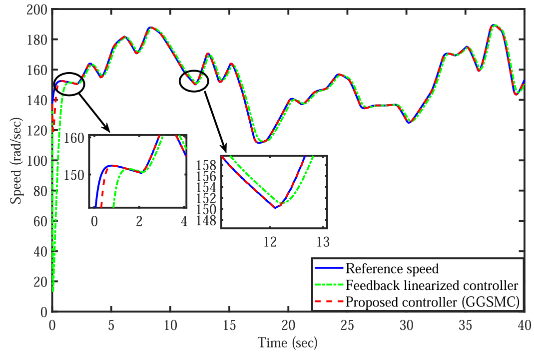

FIGURE 15. GGSMC tracking performance in comparison with results of [37].

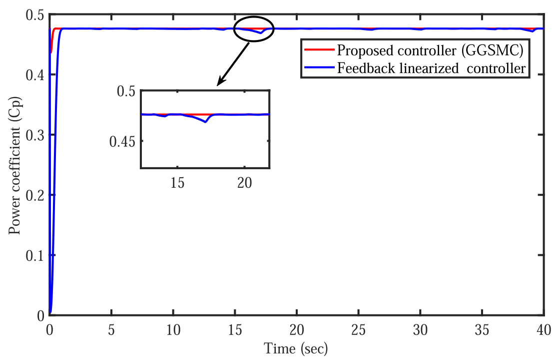

FIGURE 16. Comparison of power coefficient C_p.

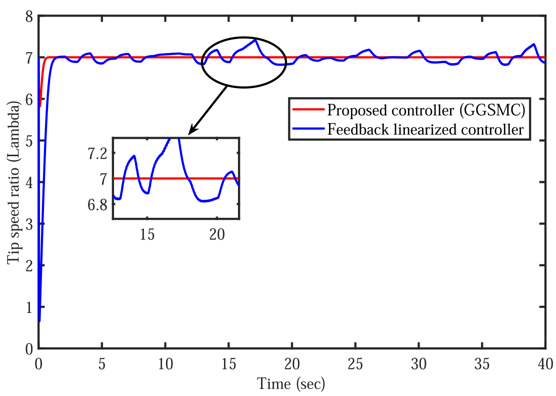

FIGURE 17. Comparison of tip speed ratio λ.

B. COMPARISON WITH STANDARD LITERATURE RESULTS

To highlight the performance of the NNs based GGSMC, its results are compared with the feedback linearized controller [37]. Both the controllers are simulated and compared with varying wind speed. Simulation results from Fig. 15-17 shows the fast tracking and better performance of the newly investigated controller as compared to the conventional feedback linearized controller. In Fig. 15, it is clearly shown that the GGSMC tracks the reference speed of the rotor in small time and have low oscillations around the reference speed as compared to the feedback linearized controller [37]. The tracking performance of both the controllers, in the fast transients, are also shown in zoomed views in the Figure. The power coefficient has its optimum value near to 0.47 which is ensured the best by GGSMC with no oscillations as compared to feedback linearized controller (one may see then in Fig. 16). The GGSMC have tip speed ratio almost around optimal tip speed ratio as compared to feedback linearized controller, as shown in Fig. 17, which guarantees maximum power extraction from the wind at the given wind speed.

Having observed the comparative results, its very clear that the FFNN based GGSMC proves its self an appealing candidate for MPPT designs in wind power systems.

VII. CONCLUSION

In this paper NNs based GGSMC MPPT law have been investigated for a variable wind speed turbine which is connected a PMSG. The unknown nonlinear dynamics (i.e., drift terms and input channels) are estimated via the FFNN and a robust GGSMC law is developed which maintain the C_p and λ at it required values and confirms maximum power extraction. The sliding mode enforcement stability is also presented in details. To highlight the benefits of the FFNN based GGSMC, its results are compared with standard literature results (i.e., feedback linearized controllers [37]). At the end it is confirmed that the newly investigated FFNN base GGSMC is an appealing candidate for such tasks in power systems.

APPENDIX

See Tables 2 and 3.

REFERENCES

[1] D. A. Dornfeld, "Moving towards green and sustainable manufacturing," *Int. J. Precis. Eng. Manuf.-Green Technol.*, vol. 1, no. 1, pp. 63–66, Jan. 2014.

[2] J. L. Sawin, F. Sverrisson, J. Rutovitz, S. Dwyer, S. Teske, H. E. Murdock, R. Adib, F. Guerra, L. H. Blanning, and V. Hamirwasia, "Renewables 2018-global status report. A comprehensive annual overview of the state of renewable energy. Advancing the global renewable energy transition-highlights of the REN21 renewables 2018 global status report in perspective," REN21, Paris, France, Tech. Rep. Renewables 2018 Global Status Report, 2018. [Online]. Available: https://www.ren21.net/wp-content/uploads/2019/08/Full-Report-2018.pdf

[3] B. Boukhezzar and H. Siguerdidjane, "Comparison between linear and nonlinear control strategies for variable speed wind turbines," *Control Eng. Pract.*, vol. 18, no. 12, pp. 1357–1368, Dec. 2010.

[4] J. Aho, A. Buckspan, J. Laks, P. Fleming, Y. Jeong, F. Dunne, M. Churchfield, L. Pao, and K. Johnson, "A tutorial of wind turbine control for supporting grid frequency through active power control," in *Proc. Amer. Control Conf. (ACC)*, Jun. 2012, pp. 3120–3131.

[5] D. Stroe, A. Stan, I. Visa, and I. Stroe, "Modeling and control of variable speed wind turbine equipped with PMSG," in *Proc. 13th World Congr. Mechanism Mach. Sci.*, Guanajuato, Mexico, 2011, pp. 19–23.

[6] C.-M. Hong, C.-H. Chen, and C.-S. Tu, "Maximum power point tracking-based control algorithm for PMSG wind generation system without mechanical sensors," *Energy Convers. Manage.*, vol. 69, pp. 58–67, May 2013.

[7] H.-W. Kim, S.-S. Kim, and H.-S. Ko, "Modeling and control of PMSG-based variable-speed wind turbine," *Electr. Power Syst. Res.*, vol. 80, no. 1, pp. 46–52, 2010.

[8] B. Beltran, T. Ahmed-Ali, and M. El Hachemi Benbouzid, "Sliding mode power control of variable-speed wind energy conversion systems," *IEEE Trans. Energy Convers.*, vol. 23, no. 2, pp. 551–558, Jun. 2008.

[9] M. Sarvi and S. Azarbara, "A novel maximum power point tracking method based on extension theory for wind energy conversion system," *Int. J. Comput. Sci. Eng. Technol.*, vol. 3, no. 8, pp. 294–303, 2012.

[10] H. Camblong, I. M. De Alegria, M. Rodriguez, and G. Abad, "Experimental evaluation of wind turbines maximum power point tracking controllers," *Energy Convers. Manage.*, vol. 47, nos. 18–19, pp. 2846–2858, Nov. 2006.

[11] S. Lalouni, D. Rekioua, K. Idjdarene, and A. Tounzi, "Maximum power point tracking based hybrid hill-climb search method applied to wind energy conversion system," *Electr. Power Compon. Syst.*, vol. 43, nos. 8–10, pp. 1028–1038, Jun. 2015.

[12] Q. Wang and L. Chang, "An intelligent maximum power extraction algorithm for inverter-based variable speed wind turbine systems," *IEEE Trans. Power Electron.*, vol. 19, no. 5, pp. 1242–1249, Sep. 2004.

[13] W. Qiao, G. Venayagamoorthy, and R. Harley, "Design of optimal PI controllers for doubly fed induction generators driven by wind turbines using particle swarm optimization," in *Proc. IEEE Int. Joint Conf. Neural Netw.*, Oct. 2006, pp. 1982–1987.

[14] M. Dorigo, L. Gambardella, M. Birattari, A. Martinoli, R. Poli, and T. Stützle, "Ant colony optimization and swarm intelligence," in *Proc. 5th Int. Workshop*, in LNCS, vol. 4150. Brussels, Belgium: Springer, 2006.

[15] M. S. Saad, H. Jamaluddin, and I. Z. Darus, "PID controller tuning using evolutionary algorithms," *Wseas Trans. Syst. Control*, vol. 7, no. 4, pp. 139–149, 2012.

[16] A. Z. Mohamed, M. N. Eskander, and F. A. Ghali, "Fuzzy logic control based maximum power tracking of a wind energy system," *Renew. Energy*, vol. 23, no. 2, pp. 235–245, Jun. 2001.

[17] R. Hilloowala and A. Sharaf, "A rule-based fuzzy logic controller for a PWM inverter in a stand alone wind energy conversion scheme," *IEEE Trans. Ind. Appl.*, vol. 32, no. 1, pp. 57–65, Jan./Feb. 1996.

[18] K. Ro and H.-H. Choi, "Application of neural network controller for maximum power extraction of a grid-connected wind turbine system," *Electr. Eng.*, vol. 88, no. 1, pp. 45–53, Nov. 2005.

[19] C. Wei, Z. Zhang, W. Qiao, and L. Qu, "An adaptive network-based reinforcement learning method for MPPT control of PMSG wind energy conversion systems," *IEEE Trans. Power Electron.*, vol. 31, no. 11, pp. 7837–7848, Nov. 2016.

[20] E. A. Bossanyi, "The design of closed loop controllers for wind turbines," *Wind Energ.*, vol. 3, no. 3, pp. 149–163, Jul. 2000.

[21] N. A. Cutululis, E. Ceanga, A. D. Hansen, and P. Sørensen, "Robust multi-model control of an autonomous wind power system," *Wind Energ.*, vol. 9, no. 5, pp. 399–419, Sep. 2006.

[22] B. Boukhezzar, L. Lupu, H. Siguerdidjane, and M. Hand, "Multivariable control strategy for variable speed, variable pitch wind turbines," *Renew. Energy*, vol. 32, no. 8, pp. 1273–1287, Jul. 2007.

[23] A. Levant, "Practical relative degree approach in sliding-mode control," in *Advances in Sliding Mode Control*. Berlin, Germany: Springer, 2013, pp. 97–115.

[24] F. Sebaaly, H. Vahedi, H. Y. Kanaan, N. Moubayed, and K. Al-Haddad, "Sliding-mode current control design for a grid-connected three-level NPC inverter," in *Proc. Int. Conf. Renew. Energies Develop. Countries*, Nov. 2014, pp. 217–222.

[25] J. Yang, S. Li, and X. Yu, "Sliding-mode control for systems with mismatched uncertainties via a disturbance observer," *IEEE Trans. Ind. Electron.*, vol. 60, no. 1, pp. 160–169, Jan. 2013.

[26] J. Li and Q. Zhang, "Fuzzy reduced-order compensator-based stabilization for interconnected descriptor systems via integral sliding modes," *IEEE Trans. Syst., Man, Cybern., Syst.*, vol. 49, no. 4, pp. 752–765, Apr. 2019.

[27] R. Gao, D. Zhai, and X. Xie, "On the design of output information-based sliding mode controllers for switched descriptor systems: Linear sliding variable approach," *Appl. Math. Comput.*, vol. 364, Jan. 2020, Art. no. 124680.

[28] J. Li and G.-H. Yang, "Fuzzy descriptor sliding mode observer design: A canonical form-based method," *IEEE Trans. Fuzzy Syst.*, early access, Jul. 22, 2019, doi: 10.1109/TFUZZ.2019.2930036.

[29] X. Yu and O. Kaynak, "Sliding-mode control with soft computing: A survey," *IEEE Trans. Ind. Electron.*, vol. 56, no. 9, pp. 3275–3285, Sep. 2009.

[30] O. Kaynak, K. Erbatur, and M. Ertugnrl, "The fusion of computationally intelligent methodologies and sliding-mode control—A survey," *IEEE Trans. Ind. Electron.*, vol. 48, no. 1, pp. 4–17, Feb. 2001.

[31] L. Shang and J. Hu, "Sliding-mode-based direct power control of grid-connected wind-turbine-driven doubly fed induction generators under unbalanced grid voltage conditions," *IEEE Trans. Energy Convers.*, vol. 27, no. 2, pp. 362–373, Jun. 2012.

[32] S. M. Mozayan, M. Saad, H. Vahedi, H. Fortin-Blanchette, and M. Soltani, "Sliding mode control of PMSG wind turbine based on enhanced exponential reaching law," *IEEE Trans. Ind. Electron.*, vol. 63, no. 10, pp. 6148–6159, Oct. 2016.

[33] C. Evangelista, P. Puleston, F. Valenciaga, and L. M. Fridman, "Lyapunov-designed super-twisting sliding mode control for wind energy conversion optimization," *IEEE Trans. Ind. Electron.*, vol. 60, no. 2, pp. 538–545, Feb. 2013.

[34] R. Errouissi and A. Al-Durra, "A novel PI-type sliding surface for PMSG-based wind turbine with improved transient performance," *IEEE Trans. Energy Convers.*, vol. 33, no. 2, pp. 834–844, Jun. 2018.

[35] C. Xia, G. Jiang, W. Chen, and T. Shi, "Switching-gain adaptation current control for Brushless DC motors," *IEEE Trans. Ind. Electron.*, vol. 63, no. 4, pp. 2044–2052, Apr. 2015.

[36] X. Hao, X. Yang, T. Liu, L. Huang, and W. Chen, "A sliding-mode controller with multiresonant sliding surface for single-phase grid-connected VSI with an LCL filter," *IEEE Trans. Power Electron.*, vol. 28, no. 5, pp. 2259–2268, May 2013.

[37] I. Munteanu, A. I. Bratcu, N. A. Cutululis, and E. Ceanga, *Optimal Control of Wind Energy Systems: Towards a Global Approach*. New York, NY, USA: Springer-Verlag, 2008.

[38] B. Boukhezzar and H. Siguerdidjane, "Nonlinear control with wind estimation of a DFIG variable speed wind turbine for power capture optimization," *Energy Convers. Manage.*, vol. 50, no. 4, pp. 885–892, Apr. 2009.

[39] V. Reyes, J. J. Rodriguez, O. Carranza, and R. Ortega, "Review of mathematical models of both the power coefficient and the torque coefficient in wind turbines," in *Proc. IEEE 24th Int. Symp. Ind. Electron. (ISIE)*, Jun. 2015, pp. 1458–1463.

[40] A. Betz, *Introduction to the Theory of Flow Machines*. Amsterdam, The Netherlands: Elsevier, 2014.

[41] Y. Soufi, S. Kahla, and M. Bechouat, "Feedback linearization control based particle swarm optimization for maximum power point tracking of wind turbine equipped by PMSG connected to the grid," *Int. J. Hydrogen Energy*, vol. 41, no. 45, pp. 20950–20955, Dec. 2016.

[42] A. Isidori, *Nonlinear Control Systems*, 3rd ed. Berlin, Germany: Springer-Verlag, 1995.

[43] M. Hagan, H. Demuth, M. Beale, and O. De Jesús, *Neural Network Design*, vol. 20. New Delhi, India: PWS Pub., 1996.

[44] R. K. Chauhan and S. Singh, "Application of neural networks based method for estimation of aerodynamic derivatives," in *Proc. 7th Int. Conf. Cloud Comput., Data Sci. Eng. Confluence*, Jan. 2017, pp. 58–64.

[45] Y. S. Lu and J. S. Chen, "Design of a global sliding mode controller for robot manipulators with robust tracking capability," *Proc. Nat. Sci. Council, Republic China, A, Phys. Sci. Eng.*, vol. 18, no. 5, pp. 463–476, 1994.

[46] F. Iov, A. D. Hansen, P. Sørensen, and F. Blaabjerg, *Wind Turbine Blockset in MATLAB/Simulink. General Overview and Description of the Models*. Aalborg, Denmark: Aalborg Univ., 2004. [Online]. Available: https://www.academia.edu/6071104/Wind_Turbine_Blockset_in_Matlab_Simulink_General_Overview_and_Description_of_the_Models

IZHAR UL HAQ received the B.S. degree in electrical electronics engineering from COMSATS University Islamabad (Abbottabad campus), Pakistan, in 2016, and the M.S. degree in electrical engineering from COMSATS University Islamabad, Pakistan, in 2019. His research interests include maximum power extraction from renewable energy systems, integration of renewable energy systems, hybrid power systems, and intelligent control of hybrid power systems.

QUDRAT KHAN (Member, IEEE) received the B.Sc. degree in mathematics and computer science from the University of Peshawar, in 2003, the M.Sc. and M.Phil. degrees in mathematics from Quaid-i-Azam University, Islamabad, in 2006 and 2008, respectively, and the Ph.D. degree in nonlinear control systems from M. A. Jinnah University, Islamabad, in November 2012. He was postgraduate scholarship holder during Ph.D., from 2008 to 2011, and IRSIP scholarship holder during PhD (as a Visiting Research Scholar at the University of Pavia, Italy). He has been working as an Assistant Professor with COMSATS, Islamabad, since July 2013. He worked as a Postdoctoral Fellow at the Department of Mechatronics Engineering, International Islamic University, Malaysia, from September 2015 to August 2016. He was selected for Young Author Support Program, IFAC, World Congress, 2011, Milan, Italy. He has published more than 50 research articles (with impact factor more than 40) in referred international journals and conference proceedings. His research interests include robust nonlinear control design, observers design, fault detection in electromechanical systems and multiagent system's control. He is listed in the young productive scientists of Pakistan in 2017 and 2018.

ILYAS KHAN works at Majmaah University, Saudi Arabia. He is currently a Visiting Professor with the Department of Mathematical Sciences, Faculty of Science, Universiti Teknologi Malaysia, Skudai, UTM Johar Bahru, Malaysia, and Faculty of Mathematics and Statistics, Ton Duc Thang University, Ho Chi Minh City, Vietnam. He is working on both analytical and numerical techniques. He has published more than 300 articles in various reputed journals. He is also the author of several books and book chapters. His research interests are Boundary layer flows, Newtonian and non-Newtonian fluids, heat and mass transfer, renewable energy, and nanofluids.

RINI AKMELIAWATI received the B.Eng. degree (Hons.) in electrical engineering from the Royal Melbourne Institute of Technology (RMIT) University, Australia, in1997, and the Ph.D. degree in electrical and electronic engineering from the University of Melbourne, Australia, in 2002. She is currently an Associate Professor with the School of Mechanical Engineering, The University of Adelaide, Australia. She was a Full Professor with the Department of Mechatronics Engineering, International Islamic University, Malaysia, from 2012 to 2018. She joined the Department as an Associate Professor, in 2008. She was a Lecturer with RMIT University, from 2001 to 2004, and Monash University, from 2004 to 2008. She is a Fellow member of Engineers Australia and a member of International Federation of Automatic Control (IFAC) Technical Committees. She was a Visiting Professor with the University of Melbourne, in 2012, and Universiti Teknologi Melaka, from 2014-2016. She has published more than 50 peer-reviewed articles in indexed journals, three books and edited books, 20 refereed book chapters, and more than 90 conference papers in international refereed conference proceedings. She has two patents in Malaysia. Her main research interests include nonlinear control systems theory and applications, intelligent and mechatronics systems, and signal and image processing. She has received more than 35 awards inform of Gold, Silver, and Bronze medals, best paper awards, best reviewer award, and other certificates from International and National organizations as well as from the university. She has been invited to be invited speaker on her research outcomes in International and National Conferences/Symposiums/Colloqiums/Seminars. In recognition of her expertise, she has been invited to review articles in prestigious international journals. She was the Vice President of the Malaysian Society of Automatic Control Engineers (MACE) (2016–2018). She was the Chair of the IEEE Instrumentation and Measurement Society Malaysia Chapter 2007–2009, the Treasurer of the same society, in 2010, and the educational executive committee, in 2016, and a secretary of the IEEE Control Systems Society Malaysia Chapter, in 2010, the Chair of Intelligent Mechatronics System Research Unit at the International Islamic University Malaysia (2010–2018). She is also the Co-Editor-In-Chief of *International Journal of Robotics and Mechatronics* (IJRM), a member of editorial advisory board of *International Journal of Intelligent Unmanned Systems* (Emerald Group, UK - since 2012), *Journal of Unmanned Systems Technology* (UNSYS Publishing, South Korea - since 2013).

KOTTAKKARAN SOOPY NISAR is currently working as an Associate Professor with the Department of Mathematics, College of Arts and Science, Prince Sattam Bin Abdulaziz University, Wadi Al-Dawaser, Saudi Arabia. His area of specialization is partial differential equations, fractional calculus, and numerical solutions for nonlinear PDEs. He has published more than 200 articles. He is also referee of several journals.

IMRAN KHAN received the B.Sc. degree in electrical engineering from the Federal Urdu University of Arts, Science and Technology, Islamabad, in 2009, the M.S. degree in electronic engineering from Mohammad Ali Jinnah University, Islamabad, in 2012, and the Ph.D. degree in electrical engineering from the Capital University of Science and Technology, Islamabad, in 2016. He is currently an Assistant Professor with the Electrical Engineering Technology Department, National University of Technology. His research interests include analysis and design of nonlinear control systems, especially sliding mode control, for various industrial applications. He has more than six years research and teaching experience.